Radio Emission from Supernova Remnants: Implications for Post-Shock Magnetic Field Amplification & the Magnetic Fields of Galaxies

Todd A. Thompson[1], Eliot Quataert[2], & Norman Murray[3,4]

[1]*Department of Astronomy and Center for Cosmology & Astro-Particle Physics, The Ohio State University, Columbus, Ohio 43210*
[2]*Astronomy Department & Theoretical Astrophysics Center, 601 Campbell Hall, The University of California, Berkeley, CA 94720*
[3]*Canadian Research Chair in Astrophysics*
[4]*Canadian Institute for Theoretical Astrophysics, The University of Toronto, 60 St. George Street, Toronto Ontario M5S 3H8*

ABSTRACT

Using observational data from the literature, we show that the non-thermal radio luminosity (L) of supernova remnants (SNRs) is a strong function of the average gas surface density (Σ_g) of the galaxy in which the remnants reside, from normal spirals to dense luminous starbursts. Our result supports the interpretation of the radio sources in M82 and Arp 220 as normal SNRs, and not "radio" supernovae. We combine a simple theory for electron cooling in SNRs with their observed radio luminosities to estimate the remnant magnetic field strength ($B_{\rm SNR}$): the correlation between L and Σ_g implies that $B_{\rm SNR}$ also increases with Σ_g. We explore two interpretations of this correlation: (1) $B_{\rm SNR}$ is generated by post-shock magnetic field amplification, with $B_{\rm SNR}^2 \propto \Sigma_g$ and (2) $B_{\rm SNR}$ results from shock-compression of the ambient interstellar medium (ISM) magnetic field ($B_{\rm ISM}$), with $B_{\rm ISM}$ being larger in denser galaxies. We find that shock compression is, on average, sufficient to produce the observed radio emission from SNRs in the densest starburst galaxies; amplification of post-shock magnetic fields is not required. By contrast, in normal spirals modest post-shock field amplification in some remnants (a factor of $\sim$ few $- 10$) is consistent with the data; we find tentative evidence that both the Alfvén speed within SNRs and the ratio of $B_{\rm SNR}^2/8\pi$ to the post-shock pressure ("ϵ_B") are constant in SNRs from galaxy to galaxy. We discuss observational tests that can be used to more definitively distinguish between these two interpretations of the radio luminosities of SNRs. Regardless of which is correct, the radio emission from SNRs provides an upper limit to $B_{\rm ISM}$ that is independent of the minimum energy assumption. For the densest starbursts, the magnetic energy density in the ISM is below the total ISM pressure required for hydrostatic equilibrium; thus magnetic fields are not dynamically important on the largest scales in starbursts, in contrast with spiral galaxies like our own. This dichotomy may have implications for galactic dynamo theory.

Key words: ISM: supernova remnants — galaxies: magnetic fields, starburst — radio continuum: galaxies

1 INTRODUCTION

The magnetic energy density of the Galaxy is in rough equipartition with both the cosmic ray and the turbulent energy densities. These components of the ISM combine to produce a midplane pressure sufficient to balance the self-gravity of the Galactic disk and thus to establish hydrostatic equilibrium (Boulares & Cox 1990). Moreover, direct probes of magnetic fields in dense star-forming regions within the Galaxy indicate that they may be dynamically important

(Crutcher 1999). Because of the potential importance of magnetic fields for star formation on small scales, at and below the scale of giant molecular clouds, and for the structure and self-regulation of galaxies on their largest scales, it is of considerable interest to understand how the average magnetic field strength varies from normal galaxies to starbursts, where the ISM conditions are considerably different.

A rough upper limit to the average magnetic field strength in a galaxy can be constructed by assuming that the field is dynamically comparable to gravity. For a thin

self-gravitating gas-dominated disk of average gas surface density Σ_g, this "equipartition" field strength is

$$B_{\rm eq} \approx 2\pi \sqrt{2G}\,\Sigma_g \approx 2.3\,\Sigma_g \ {\rm mG}, \qquad (1)$$

where Σ_g is measured in g cm^{-2}. $B_{\rm eq}$ provides an upper limit to B on galactic scales because for $B > B_{\rm eq}$ the field is buoyant and escapes the host galaxy (Parker 1966). For galaxies like the Milky Way, in which the total surface density, $\Sigma_{\rm tot}$, is dominated by stars, $B_{\rm eq}$ in equation (1) should be multiplied by a factor of $(\Sigma_{\rm tot}/\Sigma_g)^{1/2} (\approx 3)$. The measured gas surface densities of galaxies vary by more than 4 decades (e.g., Kennicutt 1998, hereafter K98). Over this range, equation (1) implies a maximum field strength of $B_{\rm eq} \approx 15\,\mu$G for the Milky Way ($\Sigma_g \approx 2 \times 10^{-3}$ g cm^{-2}; $\Sigma_{\rm tot}/\Sigma_g \approx 10$) and ~ 20 mG in galaxies like Arp 220 that anchor the high-density end of the Schmidt Law with $\Sigma_g \approx 10$ g cm^{-2} and $\Sigma_{\rm tot}/\Sigma_g \approx 1$ (Downes & Solomon 1998).

Estimates of magnetic field strengths in galaxies are traditionally limited to the "minimum energy" assumption of Burbidge (1956), which posits an equality between the magnetic and cosmic ray energy densities (see Longair 1994; Beck & Krause 2005). This approximation works well in the Galaxy and other normal spirals where the field strength is also nearly equipartition in the sense of equation (1), but the minimum energy assumption likely underestimates the field strengths in starburst galaxies because of strong cosmic ray electron cooling (Condon et al. 1991; Chi & Wolfendale 1993; Thompson et al. 2006; hereafter [T06]).

One way to see that the minimum energy estimate must fail in ultra-luminous infrared galaxies (ULIRGs) like Arp 220 is to note that the inverse Compton (IC) cooling time for radio-emitting cosmic ray electrons is $t_{\rm IC} \sim 10^4$ yr (e.g., Condon et al. 1991). The minimum energy estimate for the magnetic field strength yields a synchrotron cooling timescale at GHz frequencies that is ~ 10 times longer, and yet Arp 220 lies on the FIR-radio correlation together with essentially all star-forming galaxies (Condon 1992; Yun et al. 2001), which have synchrotron cooling times somewhat shorter than IC cooling times (e.g., Fig. 2 of T06). These facts imply that the true magnetic field strength in ULIRGs is considerably larger than the minimum energy estimate, and that rapid electron cooling invalidates the assumptions upon which that estimate is predicated.

This argument can be generalized and used to construct an empirically derived *minimum* magnetic field strength in galaxies by equating the magnetic energy density U_B and the energy density in starlight $U_{\rm ph}$. Because the ratio $U_B/U_{\rm ph}$ determines the ratio of synchrotron to IC cooling, and because normal galaxies and ULIRGs lie on *both* the FIR-radio correlation and the Schmidt Law, $U_B \equiv B^2/8\pi$ must be larger than (or a constant fraction of) $U_{\rm ph} = F/c = \epsilon\dot\Sigma_{\rm SFR}c$, where ϵ is a stellar IMF-dependent constant, F is the flux, and $\dot\Sigma_{\rm SFR}$ is the star formation rate per unit area.[1] Thus, the average magnetic field strength must exceed

---

[1] In principle, a factor of the dust optical depth should be applied to $U_{\rm ph}$ in the densest starburst galaxies, if the cosmic rays are co-spatial with the dense molecular gas that is optically thick even in the FIR (see, e.g., Thompson et al. 2005). However, this correction is uncertain and for the purposes of constructing a lower limit to B based on $U_{\rm ph}$, this expression suffices.

$$B_{\rm ph} = (8\pi\epsilon\dot\Sigma_{\rm SFR}c)^{1/2} \quad \approx \quad 0.3\,\Sigma_g^{0.7} \ {\rm mG}$$
$$\approx \quad 1.0\,\Sigma_g^{0.85} \ {\rm mG}, \qquad (2)$$

where the numerical approximations follow from the observed Schmidt Laws of K98 (top) and Bouché et al. (2007) (bottom). $B_{\rm ph}$ is a lower limit to the mean field strength in galaxies because if $U_B \lesssim U_{\rm ph}$, variations in $U_B/U_{\rm ph}$ from galaxy to galaxy would likely introduce scatter and non-linearity into the FIR-radio correlation (T06). For the Galaxy, $B \gtrsim B_{\rm ph} \approx 4\,\mu$G and for Arp 220, $B \gtrsim B_{\rm ph} \approx 1$ mG.

In this paper, we argue that radio observations of supernova remnants (SNRs) provide a complimentary probe of the ISM magnetic field strength in star-forming galaxies. In §2 we describe a simple synchrotron cooling model for the radio luminosity of an individual SNR. The radio flux depends critically on the magnetic field in the SNR, which is somewhat uncertain. At a minimum, a SNR must contain shock-compressed ISM magnetic field, which is constrained (on average) by the upper and lower limits of equations (1) and (2), respectively. However, the magnetic field in SNRs could be much stronger than the shock compressed ISM field if there is significant amplification in the post-shock plasma. We compare the remnant magnetic field strengths derived from the model presented in §2 with our expectations from equations (1) and (2), to set limits on the importance of field amplification in SNRs. We further argue that the radio emission from SNRs provides an *upper limit* on the ambient ISM field in star-forming galaxies. In §3 we show that the luminosity of SNRs is strongly correlated with the average gas surface density of the galaxy in which they reside. Using the model of §2, we invert these observations to constrain the remnant and ambient ISM magnetic field in this sample of galaxies. We discuss our results in §4, focusing on the relative importance of shock compression of ISM field versus post-shock field amplification.

2 MAGNETIC FIELDS IN SUPERNOVA REMNANTS

To estimate the radio luminosity of a SNR, we assume that a fraction $10^{-2}\xi$ of the supernova kinetic energy ($E_{51} = E_{\rm SN}/10^{51}$ ergs) is supplied to primary cosmic ray electrons in the shock and that the accelerated electrons radiate synchrotron in a magnetic field of strength $B_{\rm mG} = B/$mG. We further assume that the electron particle spectrum is flat, with a power-law index of $p = 2$ ($n(\gamma) \propto \gamma^{-p}$), as is expected theoretically for strong shocks (e.g., Blandford & Eichler 1987) and is observed *in situ* in some SN remnants (e.g., Aharonian et al. 2005; Brogan et al. 2005). A value of $\xi \approx 1$ is required to explain the integrated radio flux from star-forming galaxies, i.e., the FIR-radio correlation (Völk 1989; T06). Given the small scatter in the FIR-radio correlation (Yun et al. 2001), $\xi \approx 1$ is uncertain at the factor of $\lesssim 2$ level when averaged over many SNe in a galaxy. With these assumptions, the radio luminosity is simply (van der Laan 1962)

$$\nu L_\nu \approx \frac{\xi E_{\rm SN}}{2\ln[\gamma_{\rm max}]\,t_{\rm syn}} \approx 3\times10^{35}\xi\,E_{51}\,\nu_{\rm GHz}^{1/2}\,B_{\rm mG}^{3/2} \ {\rm ergs \ s}^{-1}, (3)$$

where $t_{\rm syn} \approx 3 \times 10^4 \ B_{\rm mG}^{-3/2} \ \nu_{\rm GHz}^{-1/2}$ yr is the synchrotron cooling timescale for electrons radiating at $\nu_{\rm GHz} = \nu/{\rm GHz}$ and where we have assumed that $t_{\rm syn} \gtrsim t_{\rm exp}$, where $t_{\rm exp}$ is the expansion time of the remnant. In the last estimate in equation (3) we have assumed $\gamma_{\rm max} = 10^6$; variations in $\gamma_{\rm max}$ from $10^4 - 10^8$ affect this estimate by only a factor of ~ 1.5.

Equation (3) is an estimate of the radio emission produced by the interaction between a SN and the ambient ISM, i.e., the emission from a SNR (e.g., Shlovskii 1960). The radio emission is expected to peak at the Sedov time and persist until the remnant cools radiatively (see the discussion of these timescales in §4). This time evolution is in contrast to *radio supernovae* which peak and decay after a month to few-years and which likely result from the interaction between a SN shock and the immediate circumstellar medium and pre-SN ejecta (e.g., Chevalier 1982; Weiler et al. 2002). Nearly all of the radio remnants discovered in M82 and Arp 220 that we discuss below do not vary appreciably on decade timescales (Kronberg et al. 2000; Rovilos et al. 2005). Rather than interpret these bright sources as *bona fide* radio SNe, we thus interpret them as normal SNRs.

Given an observed radio flux density, equation (3) can be inverted to estimate the magnetic field strength in the SNR, $B_{\rm SNR}$. Assuming that $B_{\rm SNR}$ is ambient ISM field compressed by the SN shock by a factor of $f \approx 3$ (appropriate for randomly-oriented fields; Völk et al. 2002 advocate $f \approx 6$ for young remnants), we obtain a simple estimate of the ISM magnetic field strength in terms of the SNR flux density:

$$B_{\rm ISM} \approx 3 \left(\frac{3}{f}\right)\left(\frac{D}{10\,{\rm Mpc}}\right)^{4/3}\left(\frac{S_\nu}{\rm mJy}\right)^{2/3} \xi^{-2/3} \nu_{\rm GHz}^{1/3} \ {\rm mG}, \quad (4)$$

equivalent to $B_{\rm ISM} f \approx B_{\rm SNR}$. Equation (4) is most readily interpreted as an *upper limit* on the ISM magnetic field given a set of SNRs with flux density S_ν because (1) f may be as large as ~ 7 and (2) turbulence and instabilities can in principle amplify the post-shock magnetic field. The SNR field may thus be larger than $\sim f B_{\rm ISM}$, but it is unlikely to be smaller.[2]

The assumptions made in deriving equation (4) include that $t_{\rm syn} \gtrsim t_{\rm exp}$ (weak cooling) and that $p = 2$. Together, these assumptions imply that the synchrotron spectral index should be $\alpha = (p-1)/2 = 1/2$ ($S_\nu \propto \nu^{-\alpha}$). For $p \neq 2$, and fixed total energy injected in cosmic ray electrons, the normalization of equation (4) increases, but modestly: for $p = 2.6$, $B_{\rm ISM}$ is larger by a factor of ≈ 1.5 and $B_{\rm ISM} \propto S_\nu^{5/9}$. The spectral indices of GHz radio emission from SNRs range from $\alpha \approx 0.5 - 1$ (see the refs. in Table 1). Diversity in α may signal diversity in p, evolutionary effects, that the assumption of weak cooling is violated, or some combination. Additionally, note also that $\xi \approx 1$ is not valid during the early free-expansion phase of SNR evolution.

A further assumption made in deriving equation (4) is that the supernova remnants are not radiative. If they were, f could be arbitrarily high. Indeed, Chevalier & Fransson (2001) argued that the radio point sources observed in M82 and Arp 220 are radiative, but otherwise normal, supernova remnants (i.e., not "radio" SNe). As we show below and as
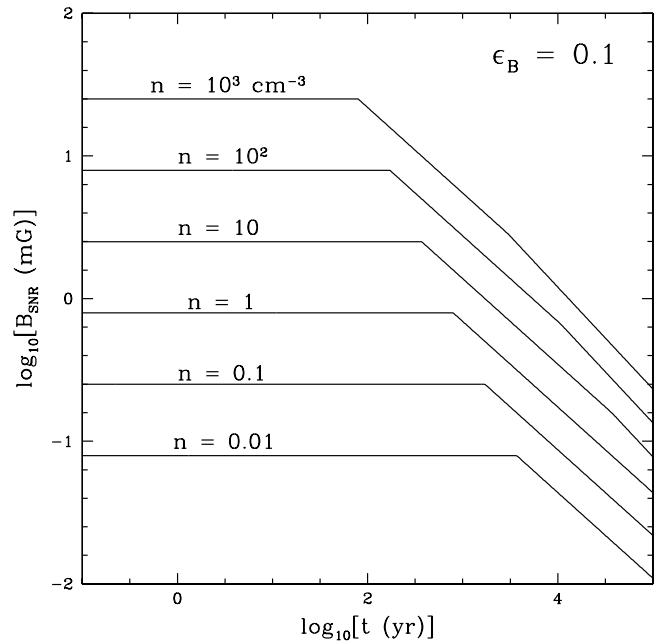
Figure 1. The time evolution of the post-shock magnetic field strength, assuming $B^2/8\pi = \epsilon_B P_{\rm sh}$, where $P_{\rm sh}$ is the post-shock thermal pressure. A 10^{51} ergs supernova shock and $\epsilon_B = 0.1$ are assumed in all cases. With these assumptions, the post-shock magnetic field is strongest during the free expansion phase, and declines during the Sedov-Taylor and snow-plow phases.

we discuss in more detail in §4, the radio luminosities of the remnants in starburst galaxies are consistent with compression of the ambient ISM magnetic field by an adiabatic shock, perhaps together with modest post-shock field amplification. Much larger f, as would be implied if the remnants were radiative, is inconsistent with independent constraints on the ambient ISM magnetic fields in these systems.

To provide some quantitative context for comparing the strength of the magnetic field in SNRs produced by flux freezing with that produced by possible amplification in the post-shock plasma, Figure 1 shows the post-shock magnetic field strength in SNRs as a function of time assuming that the post-shock remnant magnetic energy density is a factor ϵ_B times the post-shock pressure (as is often assumed in models of radio supernovae and gamma-ray burst afterglows; e.g., Reynolds & Chevalier 1981); we consider a range of ambient densities n, from low densities appropriate to SNRs in the Milky Way to high densities appropriate to SNRs in Arp 220. For these calculations we have used the analytic approximations for the evolution of SNRs developed by Draine & Woods (1991), which include both the Sedov-Taylor and pressure-driven snow-plow phases. The post-shock magnetic field is the strongest during the free expansion phase and decreases during the Sedov-Taylor phase and later as the post-shock plasma pressure decreases. We note, however, that the appropriate value for ϵ_B is quite uncertain, and thus it is difficult to estimate from first principles the importance of post-shock field amplification (see Riquelme & Spitkovsky 2009 for a recent study).

---

[2] If SNe systematically sample only low magnetic field regions of a galaxy, $B_{\rm ISM}$ inferred from SNRs may not be the same as the volume averaged magnetic field strength. This possibility cannot be ruled out, but we regard it as unlikely.
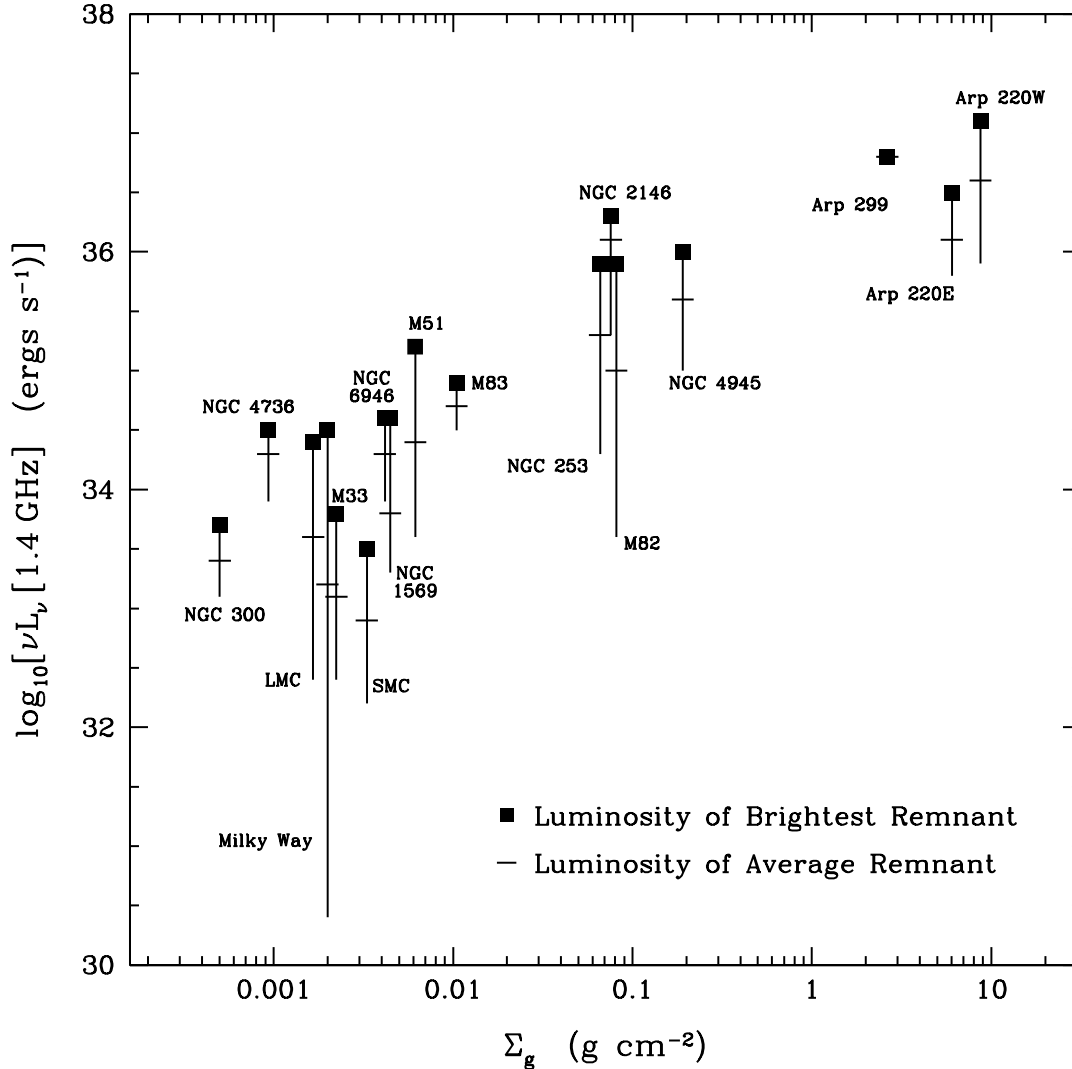
Figure 2. SNR radio luminosity versus average gas surface density, Σ_g, for the sample of star-forming galaxies in Table 1. The filled square and horizontal bar show the maximum and average SNR luminosity for each system. The vertical bar extends to the lowest SNR luminosity observed. A strong correlation is present in the data. A simple linear least squares fit to the average SNR luminosities gives $\nu L_\nu \propto \Sigma_g^{0.85}$; fitting to only the brightest remnants gives $\nu L_\nu \propto \Sigma_g^{0.78}$ (see §3; eq. 5). Note that although for some galaxies many SNRs are observed (e.g., M33 with 51 SNRs), others, like 2146, have only a handful, or in the case of Arp 299, a single confirmed SNR. For a similar figure, see Hunt & Reynolds (2006).

3 RESULTS

A large sample of radio SNRs is available in the literature. These SNRs reside in a variety of galaxies that span the full range of both the FIR-radio correlation and the Schmidt Law. In general, the remnants are identified using the VLA, MERLIN, or VLBI, and are distinguished from compact HII regions by their steep non-thermal spectra ($\alpha \gtrsim 0.5$). The few "radio SNe" proper that appear in the compilations of SNe presented in the references in Table 1 are excluded. These include remnant 41.95+57.5 in M82 from Kronberg et al. (1985) (see Kronberg et al. 2000) and SN 2000ft in NGC 7469 (Colina et al. 2001; Alberdi et al. 2006). Background objects such as AGN behind nearby galaxies like NGC 5194 are a contaminant to the SNR sample (see Table 1).

Figure 2 shows the luminosity of observed SNRs as a

function of the average gas surface density Σ_g of the galaxy in which they reside. For simplicity, all fluxes have been scaled to a frequency of 1.4 GHz assuming $\alpha = 0.5$, even in those cases where α is known empirically in some frequency range. References, assumed distance, number of remnants, maximum and average SNR luminosity, and the sensitivity, frequency, and resolution of the observations are given in Table 1. For all of the galaxies we consider, the remnants account for just a few to ten percent of the total non-thermal continuum. Each vertical line in Figure 2 is a separate galaxy (or, for Arp 220, component). The filled square shows νL_ν for the brightest single SNR. The line for each system extends to the lowest luminosity remnant identified. The horizontal line shows the average luminosity of the observed
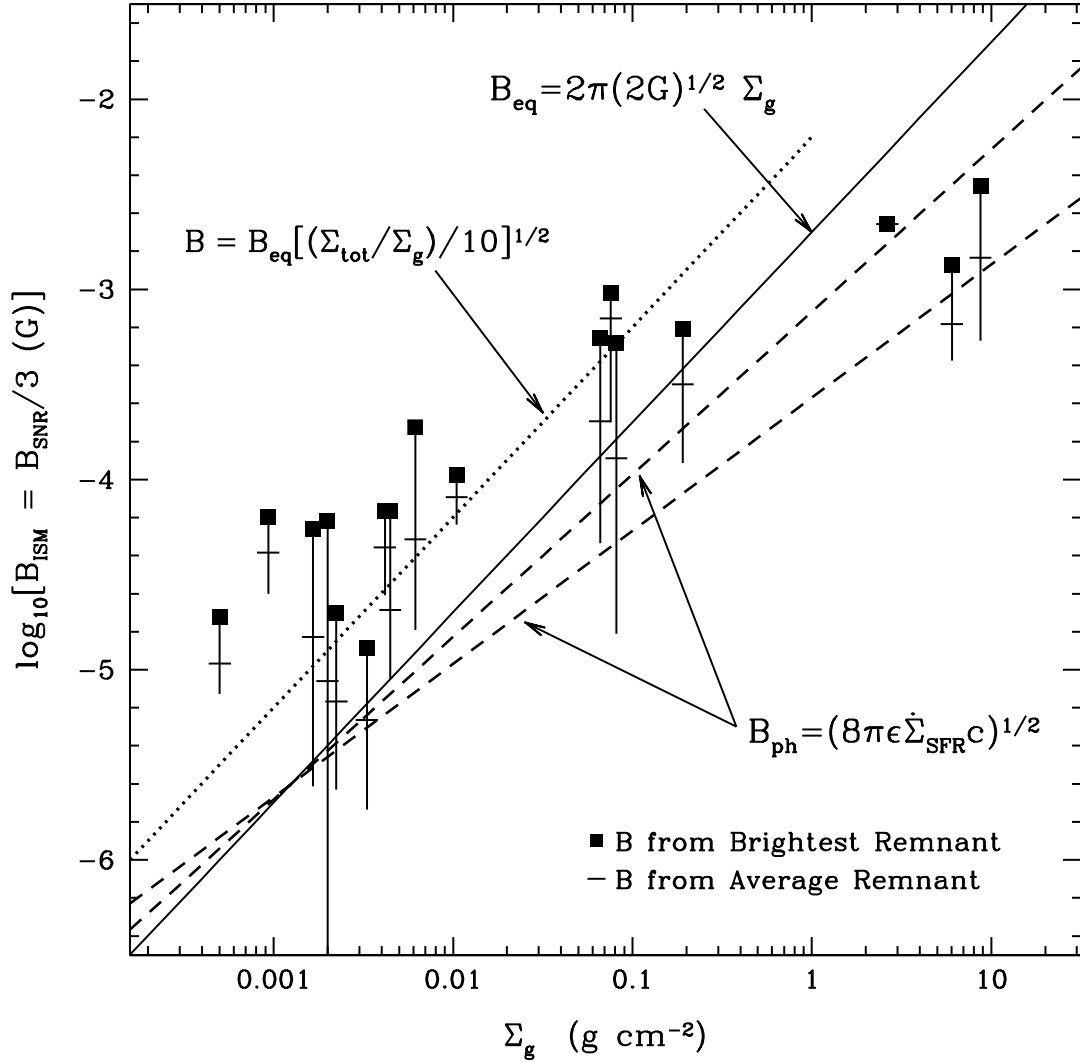
Figure 3. Inferred ISM magnetic field strength as function of Σ_g for the galaxies in Table 1 (from eq. 4 with $f = 3$), assuming that shock compression of ambient ISM field determines the magnetic field strength in SNRs (B_{SNR}); alternatively, this plot can be interpreted as showing B_{SNR}/f. As in Figure 2, the filled square and horizontal bar show the maximum and average value of B from the brightest and average SNR, for each system. The vertical bar extends to the lowest SNR luminosity observed. The thick solid line is the maximum magnetic field estimate for a gas-dominated self-gravitating disk, B_{eq} (eq. [1]). The dotted line includes the correction discussed after eq. (1) for disks that are not gas-dominated ($\Sigma_{\mathrm{tot}}/\Sigma_g = 10$). The dashed lines show the minimum required magnetic field strength for consistency with the FIR-radio correlation (see eq. 2), assuming the average Schmidt Law from K98 (shallower index) and Bouché et al. (2007) (steeper index). An unweighted linear least-squares fit to B_{ISM} or B_{SNR}, inferred from the average luminosity SNR (horizontal lines on each bar), gives $B \propto \Sigma_g^{0.56}$, whereas a fit to the brightest SNRs (highest inferred field strengths, filled squares) gives $B \propto \Sigma_g^{0.52}$ (compare with Fig. 4).

SNR distribution. A similar figure was constructed by Hunt & Reynolds (2006).

A strong correlation is evident between νL_ν and Σ_g. A simple power-law fit to the average SNR luminosities (horizontal bars) gives

$$\log_{10}\left[\frac{\nu L_\nu(1.4\,\mathrm{GHz})}{\mathrm{ergs\ s^{-1}}}\right] \approx 36.03 + 0.85\log_{10}\left[\frac{\Sigma_g}{\mathrm{g\ cm^2}}\right]. \quad (5)$$

A similar fit is found for the brightest SNRs (filled squares), but with a normalization of 36.48 and a slope of 0.78. It is also clear that the *lowest* SNR luminosities exhibit a cor-

relation with Σ_g that is qualitatively similar to that of the average and brightest SNRs.

The latter raises the concern that the results of Figure 2 may represent a selection bias rather than a physical effect. The correlation between the *maximum* SNR luminosity and Σ_g in Figure 2 is the most secure and is not subject to an obvious bias. In particular, although faint remnants in high-Σ_g galaxies (which are rarer and thus tend to be more distant) would be undetectable, bright remnants could be readily seen in nearby low-Σ_g systems, but are not. On the other hand, the correlations between the average and lowest

remnant luminosity and Σ_g are more subject to the obvious bias that faint remnants are difficult to detect in all galaxies. One might anticipate that this bias would be particularly severe for higher Σ_g galaxies and could account for the absence of low luminosity remnants in these systems. One indication that this effect does not significantly affect our calculation of the average SNR luminosity is that nearly all of the detected remnants in M82, at a distance of 3.6 Mpc, are more luminous than even the brightest remnant in NGC 300 at a distance of 1.9 Mpc (see Table 1). An additional piece of information comes from comparing the samples of Muxlow et al. (1994) with Fenech et al. (2008) for the remnants in M82. The latter are three times more sensitive than the former, and yet, comparing the two datasets we see that the average SNR luminosity decreases by just a factor of ~ 1.5, from $\log_{10}[\nu L_\nu^{\mathrm{mean}}] \approx 35.1$ to ≈ 34.9. A detailed comparison of the luminosity function of detected SNRs in all galaxies in this sample would be useful both for exploring the density and magnetic field distribution of the ISM (§4.3), and for a more detailed understanding of the selection effects at low remnant luminosity. Finally, we note that an additional reason that the *lowest* luminosity SNRs correlate with Σ_g is that detectable remnants must be brighter than the diffuse radio continuum of their host galaxy, which is larger in high-Σ_g galaxies as a result of the Schmidt Law ($\dot{\Sigma}_{\mathrm{SFR}} \propto \Sigma_g^{1.4}$; K98; $\dot{\Sigma}_{\mathrm{SFR}} \propto \Sigma_g^{1.7}$; Bouché et al. 2007) and the FIR-radio correlation.

From the observed luminosities in Figure 2, we can infer the SNR magnetic field B_{SNR} under the assumptions of equations (3) and (4). To compare this magnetic field estimate with other constraints on the ISM magnetic field, we plot these results in Figure 3 in terms of the ISM magnetic field strength $B_{\mathrm{ISM}} \equiv B_{\mathrm{SNR}}/f$, i.e., the ambient ISM field strength that would produce a SNR field strength of B_{SNR} by flux freezing. The correlation in Figure 2 combined with equation (4) implies that B_{SNR} and B_{ISM} are strong functions of Σ_g. A simple linear least-squares fit to the data points for the average SNRs (horizontal bars) gives

$$\log_{10}\left[\frac{B_{\mathrm{ISM}}}{\mathrm{G}}, \frac{B_{\mathrm{SNR}}/3}{\mathrm{G}}\right] \approx -3.20 + 0.565\log_{10}\left[\frac{\Sigma_g}{\mathrm{g\ cm^2}}\right]. (6)$$

For the brightest SNRs the relation is similar, but with normalization -2.90 and slope 0.52. Note that for larger assumed p, the correlation between B_{ISM} and Σ_g flattens (see the discussion after eq. 4). Figure 3 demonstrates that for normal spirals the magnetic field strength B_{ISM} inferred from the average-brightness SNR is comparable to or larger than the equipartition field, B_{eq} (dotted line), and larger than the minimum magnetic field strength B_{ph} (dashed line; eq. 2); this is true up to $\Sigma_g \sim 0.1$ g cm^{-2}, which characterizes starbursts such as NGC 253 and M82. For the densest, most luminous starbursts in our sample (Arp 299 and the nuclei of Arp 220), B_{ISM} is below B_{eq} and — at least for Arp 220 — comparable to B_{ph}. At the other extreme, for the lowest density systems in our sample, NGC 300 and NGC 4736, Figure 3 tentatively implies a trend of larger $B_{\mathrm{ISM}}/B_{\mathrm{eq}}$ at low Σ_g.

Because of the paucity of systems at very high Σ_g in Figures 2 and 3, we searched the literature for additional high resolution radio observations of local starbursts and ULIRGs. Unfortunately, the existing observations are not yet at sufficiently high spatial resolution to unambiguously imply that single SNRs have been detected. For example,

Momjian et al. (2006) found 10 compact radio sources in the ULIRG IRAS 17208-0014. Most have deconvolved sizes at half maximum of ~ 10 pc. At a distance of ≈ 170 Mpc ($z = 0.043$), it is unclear if these compact sources are indeed individual SNRs, rather than unresolved populations of multiple remnants. In addition, the spectral indices of these sources are unknown, and many may be bright HII regions. A single source is unresolved, with a linear scale < 4.9 pc. This is also the least luminous source with $S_\nu(1.6\,\mathrm{GHz}) = 119 \pm 45\,\mu\mathrm{Jy}$. Given the gas surface density from K98 (≈ 0.4 g cm^{-2}), this individual source would lie above the single Arp 299 remnant (see Table 1) in Figure 2 by a factor of roughly two. Similarly, recent observations of IRAS 23365+3604 and IRAS 07251-0248 have been reported by Romero-Cañizales et al. (2008). They reveal a number of compact radio components. However, because these galaxies are at distances of ≈ 230 and ≈ 360 Mpc, respectively, the resolution of the observations is again insufficient to associate individual sources with single SNRs. Comparing with the observations of the nuclear sources in Arp 220 by Lonsdale et al. (2006), we expect that the sources detected by Romero-Cañizales et al. (2008) are likely to be collections of ~ 10 SNRs per source. Higher resolution studies can confirm or exclude this possibility. Taking the sources from Romero-Cañizales et al. (2008) at face value, and estimating the gas surface density of these ULIRGs from the literature, both systems would lie significantly above the solid line (B_{eq}) in Figure 3, and they would deviate markedly from the trend seen in Figure 2.

4   DISCUSSION

Figure 2 demonstrates that SNR luminosities are a strong, and fairly continuous, function of Σ_g, the average (galaxy-wide) gas surface density of their host galaxy. There may be a change in the correlation for $\Sigma_g \gtrsim 0.1$ g cm^{-2}, but more observations of SNRs in dense starbursts are required to assess this. In the following, we consider two plausible interpretations of this data: (1) the luminosity of a SNR is significantly larger in denser galaxies because the ambient magnetic field is significantly larger (as in Fig. 3), or (2) SNRs are brighter in denser galaxies because the magnetic field in the post-shock plasma scales as $B^2/8\pi \propto \rho_{\mathrm{ISM}}v_{\mathrm{sh}}^2$ and is thus larger in galaxies with a denser ISM (larger ρ_{ISM}).

4.1   Field Amplification

Recall that B_{ph} (eq. 2, dashed lines in Fig. 3) is a *lower limit* to the true average ISM magnetic field strength because for $B < B_{\mathrm{ph}}$ IC losses dominate synchrotron losses and one expects a systematic deviation from the FIR-radio correlation at high FIR luminosities, which is not observed (T06). In addition, the magnetic field inferred from SNRs, B_{ISM} (eq. 4, points in Fig. 3) is an approximate *upper limit* to B because post-shock turbulence and instabilities can amplify magnetic fields in SNRs (Völk et al. 2002; Berezhko et al. 2006). It is striking that the upper and lower limits on B_{ISM} coincide to within a factor of few for high Σ_g starburst galaxies, particularly given the maximum equipartition magnetic fields these galaxies could support (B_{eq}, eq. 1). This correspondence implies that shock compression of B_{ISM} is sufficient to power SNR radio emission in dense starburst galaxies.
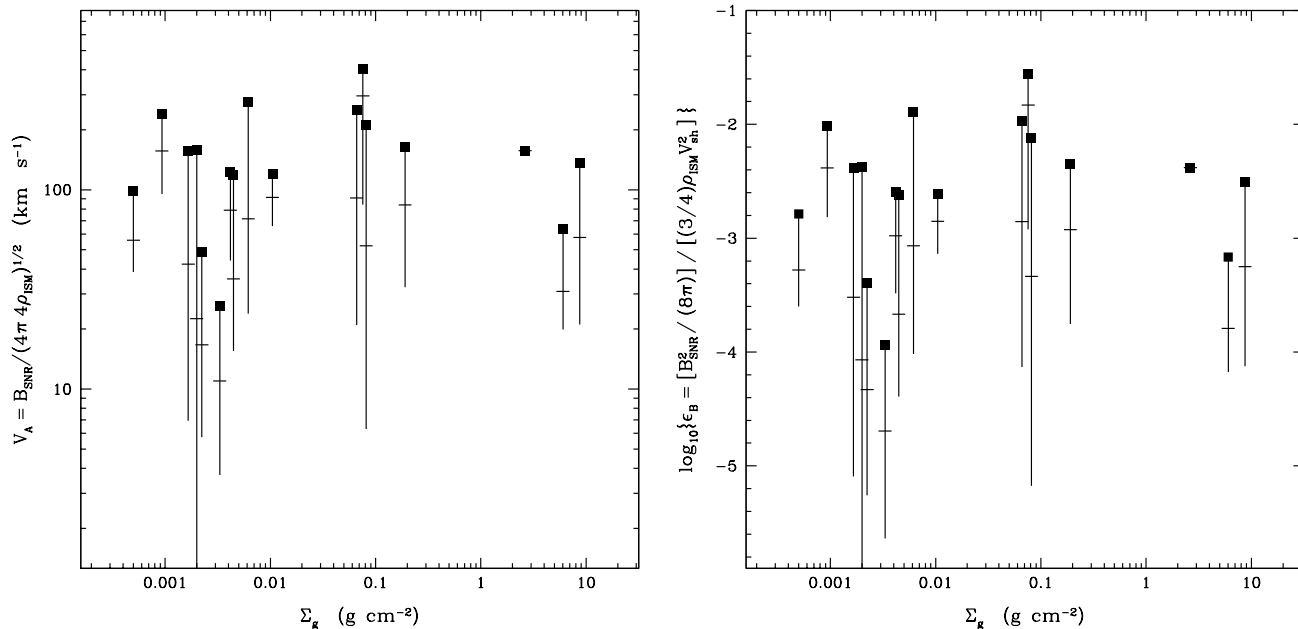
Figure 4. *Left Panel:* SNR Alfvén speed (V_A) as a function of the average ISM gas surface density Σ_g. Here, $\rho_{\rm ISM} = \Sigma_g/(2h)$, where $h = 100\,$pc is the assumed gas scale height for all galaxies. Note that the range of Σ_g plotted here corresponds to the range of average densities $0.5\ {\rm cm}^{-3} \lesssim n_{\rm ISM} \lesssim 10^4\ {\rm cm}^{-3}$. *Right Panel:* The ratio of the post-shock magnetic field energy density to the post-shock thermal pressure, $\epsilon_B = [B_{\rm SNR}^2/(8\pi)]/[(3/4)\rho_{\rm ISM}V_{\rm sh}^2]$, as a function of Σ_g for $h = 100\,$pc. In both panels, as in Figure 3, $B_{\rm SNR}$ is inferred from equation (4) and the SNR radio luminosities in Table 1. Note that if supernovae explode in regions of lower-than-average density (§4.1, §4.3), the inferred V_A and ϵ_B both increase.

For the specific case of Arp 220, our inferred ISM magnetic field strength of $\sim 1 - 3\,$mG is also reasonably consistent with the direct Zeeman detections of Robishaw et al. (2008); thus three independent observational methods, each likely probing somewhat different phases of the ISM, all imply that a magnetic field of a few mG pervades the nuclear region of Arp 220. A corollary of this is that Figure 3 provides strong evidence for the interpretation of the radio point sources in Arp 220 as normal SNRs expanding into a highly-magnetized ISM; this alleviates the need for *bona fide* radio SNe to generate the very high luminosities observed (Smith et al. 1998; Rovilos et al. 2005; Parra et al. 2007; see also Chevalier & Fransson 2001).

In contrast to starbursts like Arp 220, in normal spirals independent observations constrain the ambient ISM magnetic field to be $\sim 5 - 10\,\mu$G (e.g., Beck 1982; Fitt & Alexander 1993; Beck & Krause 2005). Compressing this field by a factor of $\sim 3 - 7$ results in a magnetic field of sufficient strength to explain the typical radio SNR observed in normal spirals (Fig. 3); it appears, however, that the brightest remnants require fields that are a factor of few larger (and perhaps more at the lowest surface densities), either because the SNe explode in a region of larger-than-average B or because of modest post-shock field amplification. Nonetheless, as in the case of starbursts, Figure 3 implies that significant post-shock magnetic field amplification (say $> \times 10$) is not required to explain the *average* radio luminosities of SNRs in spiral galaxies.

In our own Galaxy, there is some evidence for magnetic field amplification in young shell-type SNRs (e.g., Völk et al. 2002; Völk et al. 2005; Berezhko et al. 2006). In these models, individual Galactic SNRs are observed and modeled at a moment in their evolution, in contrast to the statistical approach taken here. For example, Völk et al. (2005) constrain $B_{\rm SNR} \sim 300\,\mu$G in Tycho's SNR by fitting the broadband X-ray and radio emission simultaneously. Using $\xi = 1$ in equation (4), and using only the radio data, we find that B in the remnant is $\sim 9\,\mu$G.[3] We have also compared the results from Völk et al. (2005) with our calculation for the SNRs RCW 86, SN 1006, and Cass A. We find that $B_{\rm SNR} = 3B_{\rm ISM} \approx 9$, 4, and $180\,\mu$G, whereas Völk et al. find ≈ 100, 160, $500\,\mu$G, respectively. The difference in the inferred SNR field between Völk et al. and this work lies partially in the assumptions about the energy in relativistic electrons, encapsulated in our parameter ξ in equations (3) and (4). In order to not over-produce the radio luminosity with such a large B, Völk et al. (2006) decrease the cosmic-ray electron-to-proton ratio, effectively using a small value of ξ. In contrast, the normalization of the FIR-radio correlation, which we use here to normalize the emission from all individual SNRs, requires that $\xi \simeq 1$ when averaged over a suitably large number of remnants. We expect that shock accelerated electrons will have a total energy equivalent to $\xi \simeq 1$ by the onset of the Sedov-Taylor phase, when the shocked, swept-up mass is comparable to the ejecta mass. If shock acceleration only becomes efficient very late in a remnant's evolution — or if the electrons rapidly diffuse out of the remnant on a timescale comparable to the Sedov-Taylor time — then the assumption of $\xi \simeq 1$ may be unreasonable

---

[3] This is for an adopted distance to the Tycho SNR of 2.4 kpc (from the Green catalog; see Table 1).

for a typical remnant. Although more definitive calculations are required to assess these possibilities, we regard both of them as unlikely and thus conclude that the majority of observed remnants can be interpreted assuming $\xi \simeq 1$. In this case, although individual remnants, at particular moments in time, may have fields larger than that due to compression alone, Figure 3 suggests that this is not a significant effect for SNRs in starbursts, or for the average SNR in most normal spirals.

A SNR could in principle generate magnetic fields in approximate equipartition with the post-shock thermal pressure of the gas: $B_{\rm SNR}^2/8\pi \sim \rho_{\rm ISM}v_{\rm sh}^2$ where $\rho_{\rm ISM}$ is the density of the ISM in which the SN explodes and $v_{\rm sh}$ is the velocity of the SN shock at a given time (this assumption is often used in radio SNe and γ-ray burst models; e.g., Chevalier 1982; Meszaros & Rees 1997); see Figure 1 for estimates of the magnetic field strengths in SNRs if significant post-shock field amplification indeed occurs. In this interpretation, the higher remnant luminosities in denser galaxies (Fig. 2) are due to the post-shock scaling $B_{\rm SNR} \propto \rho_{\rm ISM}^{1/2}$, rather than anything about the magnetic field in the ambient ISM.

Adopting the interpretation that post-shock magnetic field amplification is solely responsible for generating $B_{\rm SNR}$ and the observed radio emission, Figures 2 and 3 have several interesting implications. Taking a constant gas scale height of $h \approx 100$ pc for all galaxies, so that the average ISM density is $\rho_{\rm ISM} = n_{\rm ISM}m_p = \Sigma_g/(2h)$, Figure 3 implies that $B_{\rm SNR} \propto \rho_{\rm ISM}^{1/2}$, i.e., there is a constant characteristic Alfvén speed in all observed remnants.[4] The left panel of Figure 4 shows this explicitly. Here, we have plotted $V_A = B_{\rm SNR}/(4\pi 4\rho_{\rm ISM})^{1/2}$ as a function of Σ_g, assuming a constant gas scale height. A fit to the average SNRs gives

$$\log_{10}\left[\frac{V_A}{\rm km\ s^{-1}}\right] \approx 1.87 + 0.065\log_{10}\left[\frac{\Sigma_g}{\rm g\ cm^{-2}}\right]. \qquad (7)$$

For the brightest remnants, the normalization is higher (≈ 2.17) and the slope is flatter (≈ 0.021). In Figure 4, V_A is calculated assuming that the SNR density is $4\rho_{\rm ISM}$, appropriate for a strong adiabatic ($\gamma = 5/3$) shock expanding into the ISM. If, as we discuss in §4.3, supernovae tend to sample low density regions of the ISM, the implied V_A would increase, probably by a factor of $\sim 3 - 10$. Despite uncertainty in the overall normalization for V_A, the left panel of Figure 4 shows that the Alfvén speed within remnants is roughly the same for all observed SNRs in all galaxies; if magnetic field amplification is at work in SNRs, this finding is an important clue to the physics.

This result can equivalently be presented as a constraint on ϵ_B, the ratio of the post-shock magnetic energy density to the post-shock pressure (see Fig. 1). The right panel of Figure 4 shows our determination of ϵ_B for the SNRs in our sample as a function of the average ISM gas density. For the average SNRs, we find that

$$\log_{10}[\epsilon_B] \approx -3.04 + 0.131\log_{10}\left[\frac{\Sigma_g}{\rm g\ cm^{-2}}\right]. \qquad (8)$$

For the brightest remnants, the normalization is consider-

---

[4] Although the assumption of constant gas scale height across all galaxies in the sample is a reasonable first approximation, they may have systematically smaller h at higher Σ_g, which would tend to flatten the function $V_A(n_{\rm ISM})$ (see eq. 7).

ably higher (≈ -2.44) and the slope is yet flatter (≈ 0.042). The value of ϵ_B is proportional to V_A^2, so the near-constancy of ϵ_B with $n_{\rm ISM}$ is not surprising given the results for V_A in the left panel of Figure 4. As with V_A, we emphasize that the precise value of ϵ_B depends sensitively on whether or not supernovae explode in gas at the average ISM density. If, as is more likely, most of the volume is filled with gas 10 to 100 times less dense than $n_{\rm ISM}$ (§4.3), the typical inferred value of ϵ_B would be $\sim 0.01 - 0.1$.

Because the observations do not definitively favor either SN shock compression of ISM field or post-shock field amplification, we are unable to unambiguously determine which of these two possibilities is correct. An important testable difference between these two hypotheses lies in the dependence of the radio emission on shock velocity or SNR diameter $D_{\rm SNR}$. For shock compression alone, νL_ν should be independent of $v_{\rm sh}$ while if $B^2/8\pi \propto \rho_{\rm ISM}v_{\rm sh}^2$, $\nu L_\nu \propto v_{\rm sh}^{3/2}$. Another way to state this result is that the two models predict different SNR surface brightness-to-diameter relations (the $\Sigma_{\rm SNR} - D_{\rm SNR}$ relation). For shock compression alone, $\Sigma_{\rm SNR} \propto D_{\rm SNR}^{-2}$ while for $B^2 \propto v_{sh}^2$, $\Sigma_{\rm SNR} \propto D_{\rm SNR}^{-17/4}$ (in both cases assuming $p = 2$; see also, e.g., Berezhko & Völk 2004). Observations of SNRs in the Milky Way find $\Sigma_{\rm SNR} \propto D_{\rm SNR}^{-2.4}$ (Case & Bhattacharya 1998), much closer to the flux-freezing prediction, while observations of SNRs in M82 find $\Sigma_{\rm SNR} \propto D^{-3.5}$ (Huang et al. 1994), closer to the predictions of the field amplification model (see Urosević et al. 2005). For M82, the recent work by Fenech et al. (2008) finds a best fit of $\Sigma_{\rm SNR} \propto D^{-3.0}$. Updated observational samples, particularly those that characterize SNRs in high-density regions, and more sophisticated theoretical models are needed to fully understand the implications of the $\Sigma_{\rm SNR} - D_{\rm SNR}$ relation and its connection to the correlation presented in Figure 2.

4.2 The Dynamical Role of Magnetic Fields

Another important conclusion from Figure 3 is that $B_{\rm ISM} \ll B_{\rm eq}$ in the most luminous starbursts. This implies that magnetic fields are not dynamically important for hydrostatic equilibrium on large scales in these systems, in sharp contrast with spiral galaxies like our own. One possible explanation for this difference is that the lifetime of intense starbursts ($\sim 10^7 - 10^8$ yrs) is significantly shorter than that of the relatively continuous star formation in normal spiral galaxies; there may thus be less time for dynamo processes to amplify the average ISM magnetic field.

Figure 3 also suggests that the magnetic energy density U_B is comparable to the photon energy density $U_{\rm ph}$ in a wide range of systems, with $U_B \sim {\rm few} - 10\,U_{\rm ph}$, depending on the form of the Schmidt Law adopted (compare the two dashed lines in Fig. 3). This result is not as surprising as it might first appear because massive stars determine both the radiation field of galaxies and the energy and momentum injected into their ISM. The latter "feedback" can generate turbulence in the ISM, amplifying the magnetic field. Thompson et al. (2005) and Thompson (2008) have suggested a direct connection between turbulence in dense starbursts and $U_{\rm ph}$ by positing that radiation pressure from the absorption and scattering of stellar light by dust grains dominates the overall pressure support. The rapid diffusion of infrared photons in starbursts causes the medium to be gravitationally unstable (Thompson 2008) and, even in the

absence of self-gravity, generates magnetohydrodynamic instabilities that can amplify magnetic fields directly (Turner et al. 2007). In addition, the momentum supplied to the ISM by stellar winds and SN explosions is comparable to that in photons. There are thus a number of sources capable of generating turbulent motions that could amplify magnetic fields to the levels inferred here. It is also worth noting that although $B_{ph} \ll B_{eq}$ for luminous starbursts in Figure 3, this does not necessarily imply that radiation pressure is dynamically unimportant; the dense gas in starbursts is optically thick even in the far infrared and thus the energy density of photons in the densest gas is larger than that in equation (2) by a factor of the dust optical depth (see footnote 1), which can be $\sim 10 - 100$ (e.g., Thompson et al. 2005).

4.3 SNR Luminosity Function

As a final comment, we note that a more sophisticated understanding of the SNR luminosity function is needed to provide a more quantitative interpretation of the data in Figures 2 & 3. For example, although equation (3) suggests that νL_ν is independent of time, the radio luminosity of a given SNR will peak at its Sedov time and then decline when the remnant cools and the shock loses energy (the radio luminosity can decline more quickly if t_{syn} is short or if the relativistic electrons rapidly diffuse out of the remnant; see, e.g., van der Laan 1962; Baring et al. 1999; Berezhko & Völk 2004). If the average ISM magnetic field is volume-filling, and if SNe sample the medium fairly, taking an average density of Arp 220 of $\langle n \rangle \sim 10^4 \, \mathrm{cm}^{-3}$ and a SN rate of $\sim 1 \, \mathrm{yr}^{-1}$, we estimate that $\sim 10^3$ SNRs should be visible in the radio, which is at odds with the ~ 50 SNRs identified (e.g., Lonsdale et al. 2006). However, there is an important set of mitigating effects. First, calculations of high Mach number isothermal turbulence imply that for the conditions of Arp 220 the average medium is filled with gas with $n \sim 10^{-2} \langle n \rangle \approx 10^2 \, \mathrm{cm}^{-3}$ (e.g., LeMaster & Stone 2008). Second, although the synchrotron cooling time t_{syn} is longer for lower ambient density (because of an assumed smaller B_{ISM}), and one might thus expect to see more remnants, the SNRs at $t \sim t_{syn}$ are also physically larger: for $n = 10^2 \, \mathrm{cm}^{-3}$ a remnant expands to $\approx 4 \, \mathrm{pc}$ by $\sim t_{syn}$. For Arp 220, this is large enough that the SNRs would overlap on the sky and be resolved out by current VLBI observations. The radio luminosity function of SNRs is thus a convolution of the spatial variation of the ISM conditions into which SNe explode (e.g., variations in ρ_{ISM} and B_{ISM}), the time-dependence of an individual remnant, and the sensitivity and resolution of the observation. A careful study of these effects might provide important constraints on the nature of the ISM — the statistics of the density field and its magnetization — in external galaxies. In addition, it would more quantitatively determine the importance of post-shock magnetic field amplification in SNRs, and how the average (or maximum) SNR luminosity is related to the host galaxy's volume-averaged ISM magnetic field strength.

ACKNOWLEDGMENTS

REFERENCES

Aharonian, F., et al. 2005, A&A, 437, L7
Alberdi, A., Colina, L., Torrelles, J. M., Panagia, N., Wilson, A. S., & Garrington, S. T. 2006, ApJ, 638, 938
Allen, M. L., & Kronberg, P. P. 1998, ApJ, 502, 218
Baring, M. G., Ellison, D. C., Reynolds, S. P., Grenier, I. A., & Goret, P. 1999, ApJ, 513, 311
Beck, R. 1982, A&A, 106, 121
Beck, R., & Krause, M. 2005, Astronomical Notes, 326, 414
Bender, R., et al. 2005, ApJ, 631, 280
Berezhko, E. G., & Völk, H. J. 2004, A&A, 427, 525
Berezhko, E. G., Ksenofontov, L. T., Völk, H. J. 2006, A&A, 452, 217
Blandford, R., & Eichler, D. 1987, Phys. Rep., 154, 1
Bouché, N., et al. 2007, ApJ, 671, 303
Boulares, A., & Cox, D. P. 1990, ApJ, 365, 544
Brogan, C. L., et al. 2005, ApJL, 629, L105
Burbidge, G. R. 1956, ApJ, 124, 416
Case, G. L., & Bhattacharya, D. 1998, ApJ, 504, 761
Chevalier, R., A., 1982, ApJ, 259, 302
Chevalier, R. A., & Fransson, C. 2001, ApJL, 558, L27
Chi, X., & Wolfendale, A. W. 1993, Nature, 362, 610
Chomiuk, L., & Wilcots, E. 2009, arXiv:0901.2919
Christopher, M. H., et al. 2005, ApJ, 622, 346
Colina, L., Alberdi, A., Torrelles, J. M., Panagia, N., & Wilson, A. S. 2001, ApJL, 553, L19
Condon, J. J., et al. 1991, ApJ, 378, 65
Condon, J. J. 1992, ARAA, 30, 575
Crutcher, R. M. 1999, ApJ, 520, 706
Downes, D., & Solomon, P. M. 1998, ApJ, 507, 615
Draine, B. T., & Woods, D. T. 1991, ApJ, 383, 621
Duric, N., & Dittmar, M. R. 1988, ApJL, 332, L67
Fenech, D. M., Muxlow, T. W. B., Beswick, R. J., Pedlar, A., & Argo, M. K. 2008, MNRAS, 391, 1384
Filipović, M. D., Payne, J. L., Reid, W., Danforth, C. W., Staveley-Smith, L., Jones, P. A., & White, G. L. 2005, MNRAS, 364, 217
Fitt, A. J., & Alexander, P. 1993, MNRAS, 261, 445
Gallimore, J., Baum, S., & O'Dea, C. 2004, ApJ, 613, 794
Gieren, W., Pietrzyński, G., Soszyński, I., Bresolin, F., Kudritzki, R.-P., Minniti, D., & Storm, J. 2005, ApJ, 628, 695
Gordon, S. M., et al. 1999, ApJS, 120, 247
Greve, A., Tarchi, A., Hüttemeister, S., de Grijs, R., van der Hulst, J. M., Garrington, S. T., & Neininger, N. 2002, A&A, 381, 825
Greve, A., Neininger, N., Sievers, A., & Tarchi, A. 2006, A&A, 459, 441
Ho, L. C., & Ulvestad, J. S. 2001, ApJS, 133, 77
Huang, Z. P., et al. 1994, ApJ, 424, 114
Hunt, L., & Reynolds, S. 2006, Astron. Nach., 327, 448
Hyman, S. D., et al. 2000, AJ, 119, 1711
Israel, F. P. 1988, A&A, 194, 24

Israel, F. P. 1997, A&A, 328, 471

Kennicutt, R. C., Jr. 1998, ApJ, 498, 541 (K98)

Kronberg, P. P., et al. 2000, ApJ, 535, 706

Lemaster, M. N., & Stone, J. M. 2008, ApJL, 682, L97

Lenc, E., & Tingay, S. J. 2008, arXiv:0811.0057

Longair, M. S. 1994, High Energy Astrophysics (2nd ed.; Cambridge: Cambridge Univ. Press)

Lonsdale, C. J., et al. 2006, ApJ, 647, 185

Maddox, L. A., et al. 2006, AJ, 132, 310

Maddox, L. A., et al. 2007, AJ, 133, 2559

Mathewson, D. S., et al. 1983, ApJS, 51, 345

Mathewson, D. S., Ford, V. L., Dopita, M. A., Tuohy, I. R., Mills, B. Y., & Turtle, A. J. 1984, ApJS, 55, 189

Mauersberger, R., Henkel, C., Wielebinski, R., Wiklind, T., & Reuter, H.-P. 1996, A&A, 305, 421

Mauersberger, R., Henkel, C., Whiteoak, J. B., Chin, Y.-N., & Tieftrunk, A. R. 1996, A&A, 309, 705

Meszaros, P., & Rees, M. J. 1997, ApJ, 476, 232

Momjian, E., Romney, J. D., Carilli, C. L., & Troland, T. H. 2006, ApJ, 653, 1172

Muxlow, T. W. B., Pedlar, A., Wilkinson, P. N., Axon, D. J., Sanders, E. M., & de Bruyn, A. G. 1994, MNRAS, 266, 455

Neff, S. G., Ulvestad, J. S., & Teng, S. H. 2004, ApJ, 611, 186

Pannuti, T. G., Duric, N., Lacey, C. K., Goss, W. M., Hoopes, C. G., Walterbos, R. A. M., & Magnor, M. A. 2000, ApJ, 544, 780

Parra, R., et al. 2007, ApJ, 659, 314

Parker, E. N. 1966, ApJ, 145, 811

Payne, J. L., Filipović, M. D., Pannuti, T. G., Jones, P. A., Duric, N., White, G. L., & Carpano, S. 2004, A&A, 425, 443

Read, A. M., Ponman, T. J., & Strickland, D. K. 1997, MNRAS, 286, 626

Reynolds, S. P., & Chevalier, R. A. 1981, ApJ, 245, 912

Riquelme, M. A., & Spitkovsky, A. 2008, arXiv:0810.4565

Robishaw, T., Quataert, E., & Heiles, C. 2008, ApJ, 680, 981

Romero-Cañizales, C., Ángel Pérez-Torres, M., & Alberdi, A. 2008, arXiv:0812.0760

Rovilos, E., et al. 2005, MNRAS, 359, 827

Shklovskii, I. S. 1960, Soviet Astronomy, 4, 243

Smith, H. E., et al. 1998, ApJL, 493, L17

Tarchi, A., et al. 2000, A&A, 358, 95

Thompson, T. A., Quataert, E., & Murray, N. 2005, ApJ, 630, 167

Thompson, T. A., et al. 2006, ApJ, 645, 186 (T06)

Thompson, T. A. 2008, ApJ, 684, 212

Troland, T. H., & Heiles, C. 1986, ApJ, 301, 339

Turner, N., Quataert, E., & Yorke, H. 2007, ApJ, 662, 1052

Ulvestad, J. S., & Antonucci, R. R. J. 1991, AJ, 102, 875

Ulvestad, J. S., & Antonucci, R. R. J. 1997, ApJ, 488, 621

Urošević, D., et al. 2005, A&A, 435, 437

van der Laan, H. 1962, MNRAS, 124, 125

Vlemmings, W. H. T. 2008, arXiv:0804.1141

Voelk, H. J. 1989, A&A, 218, 67

Völk, H. J., Berezhko, E. G., Ksenofontov, L. T., & Rowell, G. P. 2002, A&A, 396, 649

Völk, H. J., Berezhko, E. G., & Ksenofontov, L. T. 2005, A&A, 433, 229

Weiler, K. W., et al. 2002, ARAA, 40, 387

Weiß, A., Neininger, N., Hüttemeister, S., & Klein, U. 2001, A&A, 365, 571

Wills, K. A., et al. 1997, MNRAS, 291, 517

Yun, M., Reddy, N., & Condon, J. 2001, ApJ, 554, 803

Table 1. Radio Emission from Supernova Remnants

System Name	D^a (Mpc)	$N_{\mathrm{SNR}}{}^b$	$\Sigma_g{}^c$ (g cm^{-2})	$\log[\nu L_\nu^{\mathrm{mean}}]^{\,d}$ (1.4 GHz) (ergs s^{-1})	$\log[\nu L_\nu^{\mathrm{max}}]^{\,e}$ (1.4 GHz) (ergs s^{-1})	Freq.^{f} (GHz)	Beam^g	Sensitivity^h	Refs. SNRs	Refs. Σ_g
NGC 300	1.9^p	17	0.00050	33.4	33.7	1.45	$4.7'' \times 3.6''$	$60\,\mu$Jy	1	2
NGC 4736	4.4	10	0.00093	34.3	34.5	1.45	$\ldots^q$	$\ldots^q$	3	3
LMC	0.053	21	0.0017^i	33.6	34.4	0.48	$4'.3$	few mJy	4,5	6
Milky Way	$\ldots^n$	38°	0.0020	33.2	34.5	$\ldots$	$\ldots$	$\ldots$	7	8
M33	0.84	51	0.0022	33.1	33.8	1.42	$7''$	$50\,\mu$Jy	9	10
SMC	0.065	23	0.0033^j	32.9	33.5	2.37	$40''$	0.4 mJy	11	6
NGC 6946	5.6	15	0.0042	34.3	34.6	1.4	$2''$	$20\,\mu$Jy	12	10
NGC 1569	2.2^s	23	0.0044	33.8	34.6	1.49	$1.4'' \times 1.4''$	$21\,\mu$Jy	13	10
M51	6.5	37	0.0062	34.4	35.2	1.4	$1.50'' \times 1.21''$	$22.5\,\mu$Jy	14	10
M83	7.3	4	0.011	34.7	34.9	1.4	$3.5'' \times 3.5''^r$	$45\,\mu$Jy^r	15	10
NGC 253	3.2	11	0.067^k	35.3	35.9	5.0	$0.6'' \times 0.3''$	$40\,\mu$Jy	16	10,17
NGC 2146	14.5	3	0.076	36.1	36.3	1.6	$0.19'' \times 0.15''$	$35\,\mu$Jy	18	10,19
M82	3.6	37	0.081^l	34.9	35.9	5.0	$35-50$ mas	$17\,\mu$Jy	20	21
NGC 4945	3.8	8	0.19^m	35.6	36.0	2.3	$16-15$ mas	$75\,\mu$Jy	22	23
Arp 299	41	1	2.6	36.6	36.6		5.6 mas $\times 4.5$ mas	$35\,\mu$Jy	24	10
Arp 220E	78	20	6.0	36.1	36.5	1.65	5.9 mas $\times 2.7$ mas	$5-6\,\mu$Jy	25	26
Arp 220W	78	29	8.7	36.6	37.1	1.65	5.9 mas $\times 2.7$ mas	$7-9\,\mu$Jy	25	26

^{a}Distance in Mpc.

^{b}Number of supernova remnants.

^{c}Average gas surface density.

^{d}Mean SNR luminosity. Each SNR luminosity is calculated assuming $F_\nu \propto \nu^{-0.5}$.

^{e}Maximum SNR luminosity.

^{f}Frequency of quoted flux density in SNR reference used to calculate SNR luminosity.

^{g}Measure of beamsize quoted in SNR reference.

^{h}Measure of sensitivity quoted in SNR reference. Typically RMS sensitivity per beam.

^{i}Calculated using a total gas mass of 6×10^8 M$_\odot$ (Israel 1997) and $R_{25} \approx 4.9$ kpc.

^{j}Calculated using a total gas mass of 4.5×10^8 M$_\odot$ (Israel 1997) and $R_{25} \approx 3.0$ kpc.

^{k}Surface density scaled to K98, but with the X_{CO} conversion factor advocated in Mauersberger et al. (1996a).

^{l}Total gas mass of starburst region 2.3×10^8 M$_\odot$ (Weiss et al. 2001), with diameter ≈ 870 pc, adjusted for $D = 3.6$ Mpc.

^{m}Total gas mass within a radius of $12''(\approx 221$ pc at $D = 3.8$ Mpc) is taken as 1.5×10^8 M$_\odot$ (Mauersberger et al. 1996b).

^{n}All distances from Green (2006); see also Case & Bhattacharya (1998).

^{o}From Green catalog. Only "S"-type sources with unambiguous distances are included. For comparison, using a sub-sample of the 20 SNRs from Case & Bhattacharya (1998) that overlap with the Green catalog, we have compared the highest and average SNR luminosities using distances from the former and the latter, respectively. Both the highest SNR luminosity (Cass A) and the average SNR luminosity are unchanged: $\log_{10}[\nu L_\nu^{\mathrm{mean}}(1.4\,\mathrm{GHz};\mathrm{ergs\ s}^{-1})] \approx 34.5$ and ≈ 33.5, respectively. However, for the full Green catalog of 38 sources (listed above), $\log_{10}[\nu L_\nu^{\mathrm{mean}}(1.4\,\mathrm{GHz};\mathrm{ergs\ s}^{-1})]$ decreases to 33.2, a factor of ≈ 2.0 lower than the smaller sample of Case & Bhattacharya (1998).

^{p}Distance from Gieren et al. (2005).

^{q}Values not listed in reference.

^{r}See Maddox et al. (2006), their Table 1. The four sources listed are those with confirmed optical counterparts.

^{s}Distance from Israel (1988).

References: (1) Pannuti et al. (2000); see also Payne et al. (2004); (2) Read et al. (1997); (3) Duric & Dittmar (1988); (4) Mathewson et al. (1983); (5) Mathewson et al. (1984); (6) Israel (1997); (7) fluxes from Green, D. (2006) (see http://www.mrao.cam.ac.uk/surveys/snrs/); see also Case & Bhattacharya (1998); (8) Boulares & Cox (1990); (9) Gordon et al. (1999); (10) K98; (11) Filipović et al. (2005); (12) Hyman et al. (2000); (13) Chomiuk & Wilcots (2009); see also Greve et al. (2002); (14) Maddox et al. (2007), including all sources steeper than $\alpha = 0.4$, excluding sources 53 (the nucleus) and 104 (background; Ho & Ulvestad 2001); (15) Maddox et al. (2006); (16) Ulvestad & Antonucci (1997), see also Ulvestad & Antonucci (1991); (17) Mauersberger et al. (1996a); (18) Tarchi et al. (2000); (19) Greve et al. (2006); (20) Fenech et al. (2008), but see also Kronberg et al. (1985), Huang et al. (1994), Muxlow et al. (1994); Wills et al. (1997), and Allen & Kronberg (1998); (21) Weiss et al. (2001); (22) Lenc & Tingay (2008) (23) Mauersberger et al. (1996b); (24) Neff et al. (2004); (25) Lonsdale et al. (2006), and see also Rovilos et al. (2005), Parra et al. (2007); (26) Downes & Solomon (1998)